Energy Conversion and Management 66 (2013) 98–105

Contents lists available at SciVerse ScienceDirect

Energy Conversion and Management

journal homepage: www.elsevier.com/locate/enconman

Experimental analysis of peak power output of a thermoelectric liquid-to-liquid generator under an increasing electrical load resistance

Frédéric J. Lesage [a,*], Nicolas Pagé-Potvin [b]

[a] Cégep de l'Outaouais, 333 Boul. de la Cité-des-Jeunes, Gatineau, Canada J8Y 6M4
[b] École de technologie supérieure, 1100 Rue Notre-Dame Ouest, Montréal, Canada H3C 1K3

ARTICLE INFO

Article history:
Received 11 August 2012
Received in revised form 1 October 2012
Accepted 10 October 2012
Available online 23 November 2012

Keywords:
Thermoelectric generator
Waste-heat recovery
Thermal conversion
Electrical load resistance
Load matching

ABSTRACT

Recent progress in thermoelectric power production using Bismuth Telluride Bi_2Te_3 semiconductor modules has revealed the potential to effectively convert large volumes of low temperature industrial waste-heat to electricity. In order to render the process more cost effective, greater understanding of the effects of external influences on the module's power output is necessary. Such an understanding would facilitate the design of thermoelectric generators which serve to exploit available waste-heat. To this end, an experimental study is performed on the most adjustable operating parameter on a thermoelectric liquid-to-liquid generator, the electrical load resistance. A test stand apparatus is built applying a temperature gradient on commercially available Bi_2Te_3 thermoelectric modules by means of an injection and a rejection of heat brought upon by counter current hot and cold liquids. The thermoelectric power production relative to an increasing electrical load is investigated by means of an analysis of experimentally measured results in which the thermal input conditions are varied. The results detail the thermoelectric characteristics of a liquid-to-liquid generator under an increasing electrical load resistance by identifying the optimal electrical load resistance for peak thermoelectric production. A correlation between peak thermoelectric power and thermal input conditions is presented as well as an investigation into the validity of electrical load matching.

1. Introduction

Thermoelectric modules are now being considered in a variety of power generation applications in which the caloric resource is waste-heat from processes such as pulp and paper production, data centre cooling systems and engine exhaust. In such considerations, the goal is to generate electricity from low-grade waste-heat that is within a temperature range of 25–225 °C. In this range, the semiconductor Bismuth Telluride (Bi_2Te_3) has been shown [1–3] to be the most effective commercially available thermoelectric material for exploiting the thermoelectric phenomenon known as the Seebeck effect. For this reason, many studies on low temperature applications of thermoelectric power generation investigate the properties of Bi_2Te_3 thermoelectric modules [4–6].

Generally, thermoelectric power generation aims to exploit low cost heat sources [7–9]. For example, [10–12] detail the potential use of thermoelectric modules in automotive waste-heat recovery, [13] demonstrate the use of thermoelectric materials in converting biomass cookstove waste-heat to electricity, and [14] investigate the harnessing of solar energy by coupling thermoelectric modules with concentrator lenses. In such applications, variable operating conditions imply variable thermal input conditions. It is commonly argued that such dynamic systems require a varying electrical load for optimal power output; indeed, [15] describe the importance of electrical load matching under dynamic thermal conditions in exhaust waste-heat recovery applications. Similarly, [16] discuss the importance of electrical load matching due to changing thermal conditions for a generic low temperature thermoelectric power generation system. This entails that an application in which the working conditions vary greatly, such as an automotive exhaust recovery application or a solar energy harvesting apparatus, requires a varying electrical load resistance shifting according to fluctuations in thermal conditions in an effort to maximize the thermoelectric power output. The adjustment in the electrical load resistance that is necessary when thermal conditions change is attributed to electrical load matching with the internal electrical resistance of the generator and is referred to as Maximum Power Point Tracking (MPPT). Indeed, by using Bi_2Te_3 modules to convert low grade thermal energy from liquid metal to electricity and by performing the same test under two different loads, [17] illustrated that the electrical load influences the output voltage in thermoelectric power generation. This implies that there exists an optimal load resistance. However, under varying thermal conditions, [17] did not adjust the electrical load for peak power production and

* Corresponding author. Tel.: +1 819 770 4012; fax: +1 819 770 8167.
E-mail addresses: Frederic.Lesage@cegepoutaouais.qc.ca (F.J. Lesage), nicolas.pagepotvin@gmail.com (N. Pagé-Potvin).

0196-8904/$ - see front matter © 2012 Elsevier Ltd. All rights reserved.
http://dx.doi.org/10.1016/j.enconman.2012.10.001

Nomenclature

Symbol	Description (Unit)
A	contact area of a thermocouple pellet (m^3)
H	hot side (–)
C	cold side (–)
c_p	specific heat at constant pressure (J/kg K)
I	electrical current (A)
k	thermal conductivity (W/m K)
L	length of a thermocouple (m)
max	maximum (–)
N	number of thermocouples (–)
oc	open circuit (–)
opt	optimal (–)
P	power (W)
q	heat transfer rate (W)
R_L	electrical load resistance (Ω)
R_{int}	internal electrical resistance (Ω)
T	temperature (K)
V	voltage (A)
v	fluid velocity (m/s)
$\alpha_{p,n}$	Seebeck coefficient (V/K)
ρ	electrical resistivity (Ω m)

therefore did not examine the influence of a variable electrical load.

The purpose of this study is to contribute to the development of MPPT systems by evaluating the power versus electrical load response of a novel liquid-to-liquid thermoelectric generator with respect to its thermal-hydraulic-electrical performance. To this end, a reliable test facility for an experimental characterization of the effects of an increasing load resistance on thermoelectric power output is established. A temperature gradient across a series of forty thermoelectric modules is produced by the flow of hot and cold water. In particular, this study shows that under an increasing load resistance, changing thermal input conditions have negligible effects on the optimal electrical load resistance, noted $R_{L,opt}$, for power output. Secondly, a correlation is developed relating the generator's peak thermoelectric power output to thermal input conditions; the correlation shows that peak power displays exponential behavior relative to temperature and root function behavior relative to flow rates. Thirdly, it is shown that thermoelectric power is less sensitive to electrical load error when the load is greater than optimal rather than less than optimal. Finally, the present work demonstrates that the $R_{L,opt}$ for thermoelectric production under an increasing electrical load resistance is strictly less than the internal resistance of the generator for all thermal input conditions tested.

2. Thermoelectric power

The focus of this study is the thermoelectric power production of a generator relative to an increasing electrical load resistance. The relationship between thermoelectric power and its electrical load is detailed in [18,19] in which a thermoelectric module made up of N thermocouples, such as in Fig. 1, is considered.

Assuming constant and isotropic material properties and an interconnecting material Seebeck coefficient of zero, the one-dimensional heat equation with boundary conditions $T(x=0)=T_C$ and $T(x=L)=T_H$ yields the temperature profile:

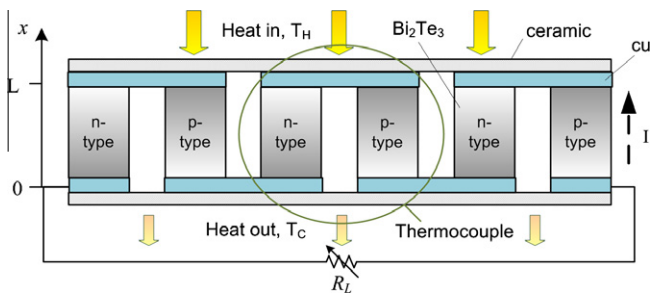

Fig. 1. Thermoelectric production from thermocouples electrically in series and thermally in parallel.

$$T = -\frac{I^2\rho}{2kA^2}x^2 + \left(\frac{I^2\rho L}{2kA^2} + \frac{\Delta T}{L}\right)x + T_c. \quad (1)$$

in which the hot and cold side temperatures are noted T_H and T_C respectively, $\Delta T = T_H - T_C$, and I is the electric currant. Energy conservation at the hot junction, $x = L$, requires that the heat flux "in" be equal to the heat flux "out" plus the energy absorbed by the Seebeck effect:

$$q_H = q_{out} - I\alpha_{p,n}T_H. \quad (2)$$

In Eq. (2), $\alpha_{p,n} = \alpha_p - \alpha_n$ is the difference in Seebeck coefficients of the p-type and n-type semiconductor pellets.

Combining Eqs. (1) and (2) with Fourier's law of conduction $q_{out} = k(2A)\frac{dT}{dx}$ at $x = L$, yields the following energy balance:

$$q_H = \frac{2kA}{L}\Delta T - \frac{I^2\rho L}{A} + I\alpha_{p,n}T_H. \quad (3)$$

Similarly, at $x = 0$, the cold side heat flux is:

$$q_C = \frac{2kA}{L}\Delta T + \frac{I^2\rho L}{A} + I\alpha_{p,n}T_C. \quad (4)$$

The power of a single module is the sum of the heat flux differences of the N thermocouples:

$$P = N(q_h - q_c) = -I^2\left(\frac{2N\rho L}{A}\right) + NI\alpha_{p,n}\Delta T. \quad (5)$$

Since the term $2N\rho L/A$ represents the sum of the electrical resistances of the thermocouples, noted the internal resistance R_{int}, Eq. (5) can be expressed as:

$$I^2R_L = -I^2R_{int} + NI\alpha_{p,n}\Delta T. \quad (6)$$

Solving for a nonzero electrical current in Eq. (6) and combining with Eq. (5) yields the power output in terms of the temperature difference and the electrical load resistance:

$$P = \frac{(N\Delta T\alpha_{p,n})^2}{R_{\text{int}} + R_L} - \frac{(N\Delta T\alpha_{p,n})^2 R_{\text{int}}}{(R_{\text{int}} + R_L)^2}. \quad (7)$$

An analysis of the above equation easily shows that the maximum power output occurs when the electrical load resistance imposed on the system is equal to the internal electrical resistance of the generator; that is to say, peak power is obtained when the electric load normalized by the internal resistance attains unity:

$$R_L^* = R_L/R_{\text{int}} = 1. \quad (8)$$

This result yielding a peak power of:

$$P_{max} = \frac{(N\Delta T\alpha_{p,n})^2}{4R_L}. \quad (9)$$

is often used when modeling peak thermoelectric power such as in the dynamic thermal conditions studied in Eakburanawat and

Boonyaroonate [20] and Crane and Bell [15]. The validity of load matching for peak thermoelectric power is investigated in the context of an increasing electrical load.

3. Experimental setup

An experimental test stand is built in order to measure power output of thermoelectric modules with an increasing electrical load resistance. The test stand supplies heat by channelling hot water between two layers of thermoelectric modules that are electrically in series while drawing heat away from the outer side of the module layers with cold water.

The central piece of the test stand is a generator consisting of two sets of twenty commercially available Bi_2Te_3 thermoelectric modules TEG2-07025HT-SS placed on either side of a hot fluid flow channel. Two cold fluid flow channels enclose the system dissipating heat thereby stabilising a temperature gradient across the modules. The result is an aluminum encased purpose built thermoelectric liquid-to-liquid generator assembled by Thermal Electronics Corp., and presented in Fig. 2.

In this way, the contrast in the hot temperature field with the cold temperature field generates a thermoelectric current known as the Seebeck effect. A thermoelectric module is made up of an assemblage of *p*–*n* junctions that are electrically in series due to the alternating *n*-type and *p*-type Bi_2Te_3 semiconductor pellets. The module assemblage is held in place with ceramics, is thermally in parallel and measures 40 mm × 40 mm × 3.75 mm.

The generator in which the modules are encased measures 47.22 cm by 9.07 cm by 1.73 cm. The hot and cold fluid flow tubes have an interior diameter of 9.52 mm and an exterior diameter of 12.70 mm and water is used as the working fluid. The hot water pipes of the generator are connected to a *MicroTherm CMX Series Temperature Control System* which is a combined pump and heating closed loop. Thermocouple temperature sensors are positioned at each fluid entry and exit. Pressure gauges are placed at the entry and exit of the hot fluid flow. Data acquisitioning of fluid temperature, fluid pressure, electrical load resistance and voltage are performed with DataStudio software in which sensor readings are relayed to the computer via the interface ScienceWorkshop 750. A carbon wire rheostat with a manual cursor is used to vary the electrical load resistance from 0 to 40 Ω. Flow turbulating inserts are placed in all fluid flow channels in an effort to improve thermal transport between the thermoelectric materials and the water. Indeed, [21] identify in a previous study that the flow turbulating inserts with alternating tabs every 7.9 mm on a 9 mm × 0.5 mm shim greatly improve power output over a large range of thermal conditions. The control system of the experimental apparatus is presented in Fig. 3. It is important to note that the hot and cold fluid flow channels are in opposing directions. This is noteworthy since it is also common – in an effort to increase the quantity of thermoelectric material used – to stack the modules in many layers as was done by [22]. However, this leads to alternating parallel and countering hot and cold fluid flow channels which differs mechanically from the test stand of the present work. In the present study, parallel flow is purposely avoided in order to favor a homogeneous temperature gradient the length of the generator.

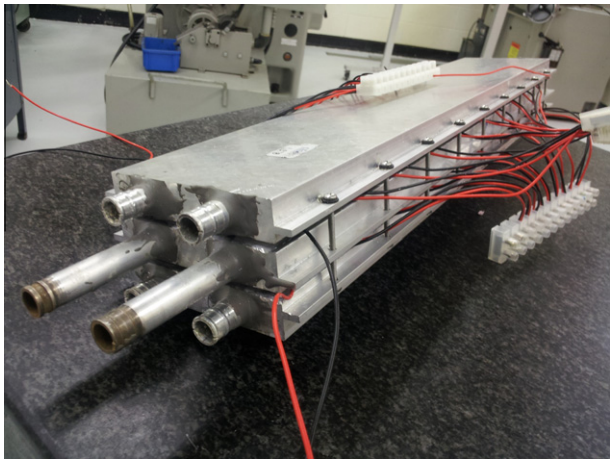

Fig. 2. Aluminum encased thermoelectric liquid-to-liquid generator.

The electrical resistances R_B, R_1, and R_2 identified in Fig. 3 are measured to be 1.0 Ω, 39.0 kΩ, and 14.8 kΩ respectively within an accuracy of 0.8% using a *BK Precision* Digital Multimeter Model 388-B. The voltage across the TEG is measured using a voltage divider setup such that:

$$V_{TEG} = V_A \frac{R_1 + R_2}{R_2}. \tag{10}$$

The thermoelectric power, noted *P*, is calculated by measuring V_A and V_B and coupling them with the measured electrical resistances of the circuit such that:

$$P = V_{TEG} I = V_{TEG} \frac{V_B}{R_B}. \tag{11}$$

Similarly, the electrical load resistance is:

$$R_L = \frac{V_{TEG}}{I} = V_{TEG} \frac{R_B}{V_B}. \tag{12}$$

The voltages V_A and V_B are measured using Science Workshop Interface to an accuracy of ±10 mV and ±3 mV respectively. In this study, the thermoelectric power output readings and the electrical load resistance readings are calculated to each have a maximum uncertainty of 3.7% for all thermal input conditions tested.

4. Results and discussion

The following test cases characterize the effects of an increasing electrical load resistance on the thermoelectric production of a liquid-to-liquid generator for varying thermal input conditions. Particular attention is placed on the electrical load resistance that yields peak power, noted $R_{L,opt}$. As such, the present study focuses on the influence that thermal conditions have on the $R_{L,opt}$ under a variable electrical load resistance.

In order to identify peak power with respect to the electrical load, the power output is normalized by the maximum power output of the specified test case such that:

$$P^* = P/P_{max}. \tag{13}$$

In this way, the maximum point on the normalized power output curves for each test case attains unity and optimal electrical loads are easily compared.

In order to investigate the thermoelectric effect under a variable electrical load, power output of the forty module liquid-to-liquid thermoelectric generator is measured under different thermal input conditions. These conditions are varied in three ways: firstly, by changing the temperature difference between the hot and cold fluids; secondly, by changing the flow rate of the hot fluid; and thirdly, by changing the flow rate of the cold fluid.

4.1. Thermal input variation due to temperature

The first set of experiments examines the effects of a change in thermal conditions by varying the hot inlet temperature. The flow rates for the hot and cold sides are maintained at 4.37 L/min and 5.00 L/min respectively, the cold fluid inlet temperature remains

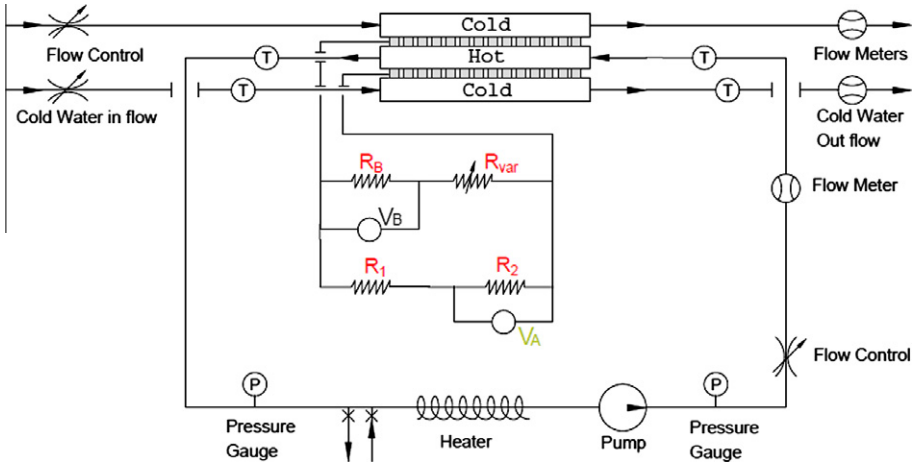

Fig. 3. Schematic representation of thermoelectric liquid-to-liquid generator experimental setup.

Table 1
Inlet and outlet temperatures for test cases of Section 4.1.

ΔT_{avg}	8.6 °C	16.4 °C	25.3 °C	33.0 °C	50.3 °C
$T_{H,in}$ (°C)	30.6	40.6	48.9	59.4	79.4
$T_{H,out}$ (°C)	29.4	40.0	46.7	58.3	75.0
$T_{C,in}$ (°C)	21.1	22.8	21.1	23.9	23.3
$T_{C,out}$ (°C)	21.7	25.0	23.9	27.8	30.6

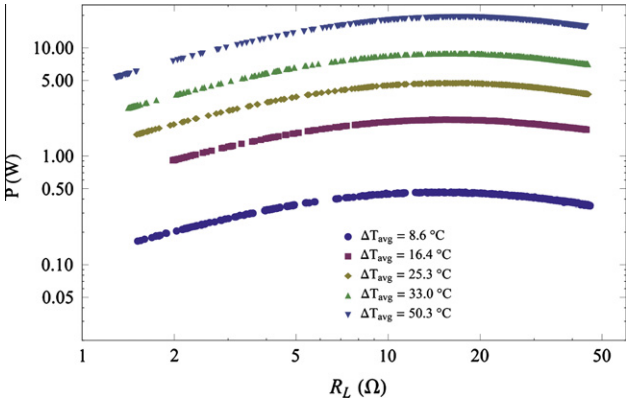

Fig. 4. Effect of an increasing electrical load resistance on power output.

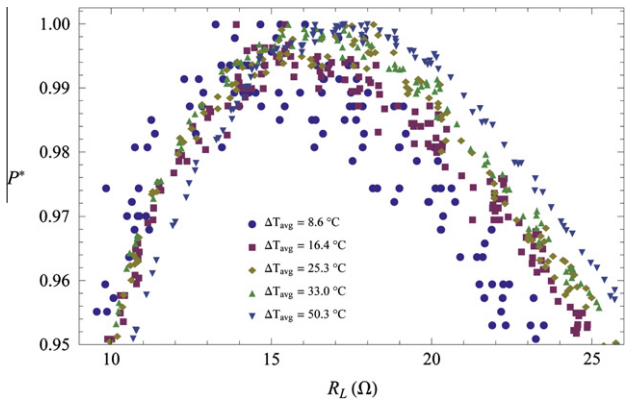

Fig. 5. Effect of an increasing electrical load resistance on normalized power output relative to ΔT.

between 21.1 and 23.9 °C, and the hot fluid inlet temperature is increased from 30.6 to 79.4 °C. The electrical load resistance is increased at a rate of 6.9 ± 2.1 Ω/s. Each test case generates a temperature difference between the heat source and the heat sink and is identified by the difference in the average cold side temperature and the average hot side temperature such that:

$$\Delta T_{avg} = (T_{H,in} + T_{H,out})/2 - (T_{C,in} + T_{C,out})/2. \quad (14)$$

It is important to note that the temperature difference across the actual modules embedded in the generator is strictly less than ΔT_{avg} due to the thermal resistance of the forced convection and the interface materials.

The temperature readings at the fluid flow inlets and outlets for each of the test cases of this section are given in Table 1.

The results illustrated in Fig. 4 show that the thermoelectric power output for all temperatures tested have similar trends. In particular, for each test case, power output increases with increasing electrical load resistance until a peak power is reached at an optimal load $R_{L,opt}$. Beyond $R_{L,opt}$, the thermoelectric power decreases more gradually. It is important to note that Fig. 4 is presented on a Logarithmic scale in order to illustrate the similar trends amongst the different test cases despite the large range in power outputs.

In Fig. 5, the power output is normalized by the maximum power obtained in each test case. It is shown that all temperature fields generate similar power output trends relative to the electrical load. More specifically, the normalized power output curves for all temperature conditions tested collapse into one curve suggesting that MPPT due to a variation in thermal conditions is not necessary relative to the electrical load resistance. Indeed, the power output for each thermal input condition is above 99.0% when within the range of all $R_{L,opt}$.

In order to illustrate the peak power and optimal load trends relative to the temperature differential, the data points of each test case are curve fit to a seventh order polynomial from which the coordinates of the maximum point are identified. The peak power and optimal load trends are illustrated in Fig. 6. Consistent with Eq. (9), the maximum power output increases with an approximate parabolic curve relative to ΔT. Conversely, despite a large change in thermal input conditions and thermoelectric power production, the $R_{L,opt}$ increases only gradually from 14.8 to 17.2 Ω. This is attributed to an increase in material internal resistance brought upon by an increase in module mean temperature; such an increase in internal electrical resistance subsequently increases the optimal electrical load.

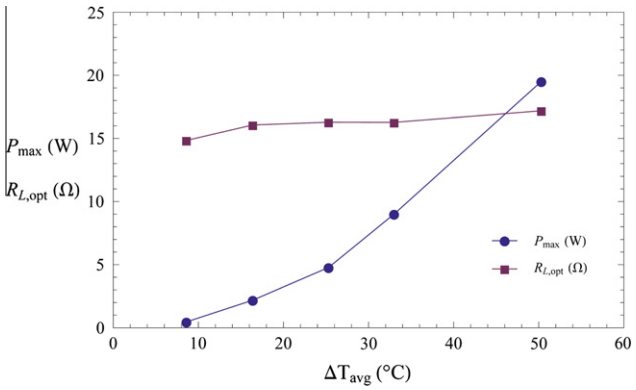

Fig. 6. Maximum thermoelectric power output and corresponding optimal electrical load resistance with respect to ΔT.

4.2. Thermal input variation due to hot flow rate

The effects of an increasing load resistance on power production for changing thermal input conditions in which the hot flow rate is varied are illustrated in Fig. 7. The hot fluid inlet temperature remains between 78.9 and 81.1 °C and the cold fluid inlet temperature remains between 20.0 and 20.6 °C. The cold fluid flow rate is maintained at 2.5 L/min for each test case and the hot fluid flow rate is increased from 0.49 to 4.37 L/min. It is important to note that the cross sectional area of the flow tubes is fixed and that any variation in flow rate corresponds to a variation in fluid velocity. The electrical load resistance is increased at a rate of 7.8 ± 2.6 Ω/s.

The temperature readings at the inlets and the outlets of the flow fluids for the test cases of this section are given in Table 2.

The normalized power output curves of Fig. 7 show that each test case experiences a sharp increase in power output until reaching a peak power at an optimal electrical load. In particular, an increase in hot fluid flow rate is not shown to have a measurable effect on $R_{L,opt}$. More specifically, for the range of $R_{L,opt}$, all test cases are above 99.6% power output.

Fig. 8 plots the peak power and optimal electrical load trends for each test case. The results differ from the observations of Section 4.1 in that the peak power curve exhibits a more linear or root function behavior rather than parabolic while the $R_{L,opt}$ curve exhibits a constant behavior. The peak power increase is attributed to an increase in convective heat transfer to the embedded thermoelectric modules thereby increasing the temperature difference across the modules. This increased temperature difference increases power exponentially in accordance to Eq. (9). The peak power linear to root function behavior is attributed to a rate of increase of thermal transport with respect to the hot flow rate that decreases with increasing flow rates. For larger flow rates, the peak power output is expected to plateau due to the fact that the upper limit of the hot side of the modules is the temperature of the hot inlet fluid.

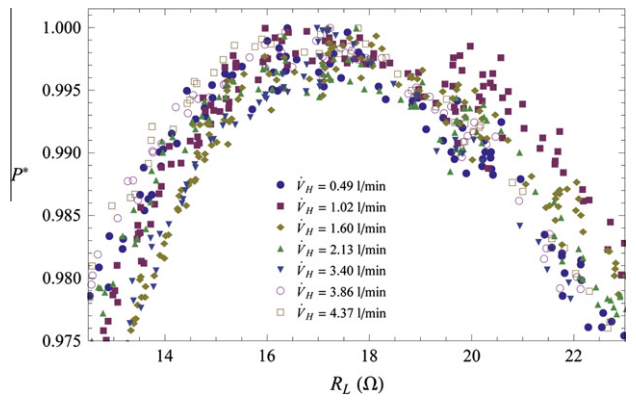

Fig. 7. Effect of an increasing electrical load resistance on normalized power output relative to hot fluid flow rate.

4.3. Thermal input variation due to cold flow rate

A third way to vary the thermal input conditions of a thermoelectric liquid-to-liquid generator is to vary the cold fluid flow rate. Fig. 9 illustrates the effects of an increasing electrical load resistance on thermoelectric power production for different cold fluid flow rates. The hot fluid inlet temperature remains between 78.3 and 79.4 °C and the cold fluid inlet temperature remains between 19.4 and 20.0 °C. The hot fluid flow rate is maintained at 2.13 L/min for each test case and the cold fluid flow rate is increased from 2.5 to 10.0 L/min. The electrical load resistance is increased at a rate of 7.8 ± 2.6 Ω/s. It is important to note that the cold fluid flow rates are larger than the hot fluid flow rates since the apparatus has four cold fluid flow channels compared to two hot fluid flow channels.

The temperature readings at the inlets and the outlets of the flow fluids for the test cases of this section are given in Table 3.

Fig. 9 illustrates the effect of an increasing electrical load on the normalized power output for these test cases. No measurable change in the $R_{L,opt}$ due to the variations in cold inlet flow rate is observed.

The results illustrated in Fig. 10 shows that peak power exhibits root function behavior with respect to the cold fluid flow rate. The increase in power output is attributed to the increase in cold fluid flow which improves the heat sink thermal transport effectively increasing the temperature difference across the embedded modules. The maximum power output curve appears as a root function relative to the cold fluid flow rate since the rate of increase of thermal transport with respect to the cold flow rate decreases with increasing flow rate. The results illustrated in Fig. 10 also show that, despite an important increase on the power output, a change in thermal conditions due to cold fluid flow rate decreases the $R_{L,opt}$. This is attributed to the increased cold fluid flow lowering the mean temperature of the modules which decreases the internal resistance of the materials thereby decreasing the optimal electrical load.

4.4. Generalized trends and thermoelectric peak power

The thermoelectric power output trends for all of the thermal input conditions tested in the previous sections are curve fit to one curve in order to illustrate its rate of change relative to the electrical load; the results are illustrated in Fig. 11.

For all thermal input conditions tested, a sharp increase in power output is produced as the electrical load approaches $R_{L,opt}$ where upon maximum power is attained. As the electrical load increases beyond $R_{L,opt}$, thermoelectric power decreases more gradually at a nearly constant rate. This implies that an MPPT should err on the side of an electrical load resistance that is greater than $R_{L,opt}$ rather than less than.

Specifically, the larger $\frac{dP^*}{dR_L}$ values for $R_L < R_{L,opt}$ imply that the power output is sensitive to small changes in R_L in this range. However, for $R_L > R_{L,opt}$, values of $\frac{dP^*}{dR_L}$ near zero are produced tending to a constant value implying that the thermoelectric power output is less sensitive to electrical loads that are greater than optimal.

In order to factor in all thermal conditions into a single non-dimensional term, x^* is defined:

Table 2
Inlet and outlet temperatures for test cases of Section 4.2.

Hot flow (°C):	0.49 L/min	1.02 L/min	1.60 L/min	2.13 L/min	3.40 L/min	3.86 L/min	4.37 L/min
$T_{H,in}$	79.4	80.6	78.9	79.4	78.9	78.9	81.1
$T_{H,out}$	57.8	62.2	68.3	71.1	72.2	73.9	75.0
$T_{C,in}$	20.0	20.0	20.0	20.0	20.6	20.6	20.6
$T_{C,out}$	30.0	30.0	32.2	32.2	32.8	32.8	32.2

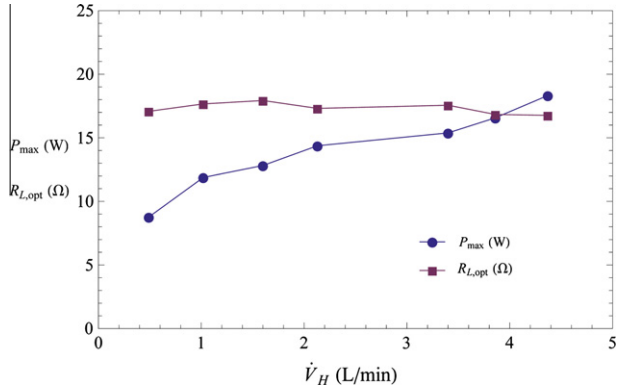

Fig. 8. Maximum thermoelectric power output and corresponding optimal electrical load resistance with respect to hot fluid flow rate.

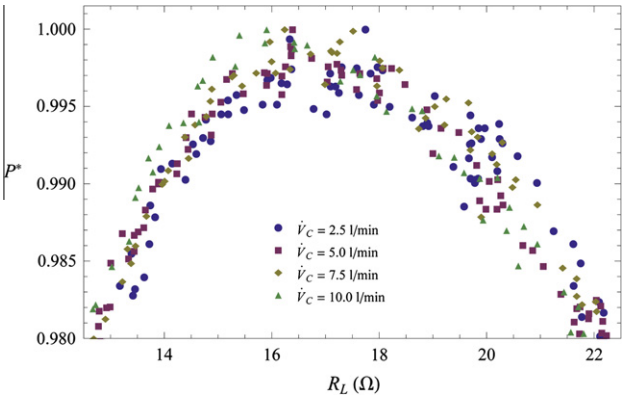

Fig. 9. Effect of an increasing electrical load resistance on normalized power output relative to cold fluid flow rate.

Table 3
Inlet and outlet temperatures for test cases of Section 4.3.

Cold flow (°C):	2.5 L/min	5.0 L/min	7.5 L/min	10.0 L/min
$T_{H,in}$	79.4	78.9	78.3	79.4
$T_{H,out}$	71.1	70.0	69.4	70.0
$T_{C,in}$	20.0	20.0	19.4	20.0
$T_{C,out}$	32.2	25.0	22.8	23.9

$$x^* = 20,200\left(\frac{v_H}{\sqrt{c_{p,H}\Delta T_{avg}}}\right)^{\frac{1}{6}}\left(\frac{v_C}{\sqrt{c_{p,C}\Delta T_{avg}}}\right)^{\frac{1}{8}}\left(\frac{\Delta T_{avg}}{T_H}\right)^{\frac{5}{2}}. \quad (15)$$

in which v_H and v_C are the hot and cold side fluid velocities.

The first two terms on the right side of Eq. (15) are Eckert numbers. Their numerators represent the kinetic energy of the fluid flows while their denominators represent the hot and cold side enthalpy differences; The last term on the right side of Eq. (15) is the Carnot efficiency. It is duly noted that the non-dimensional term x^* of Eq. (15) is a root function with respect to the fluid flow and an exponential function with respect to the temperature difference.

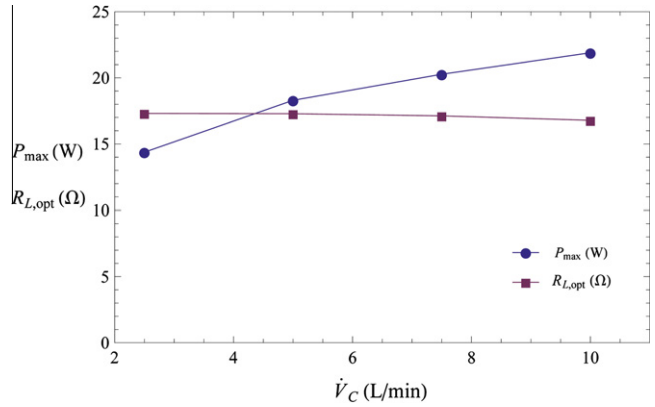

Fig. 10. Maximum thermoelectric power output and corresponding optimal electrical load resistance with respect to cold fluid flow rate.

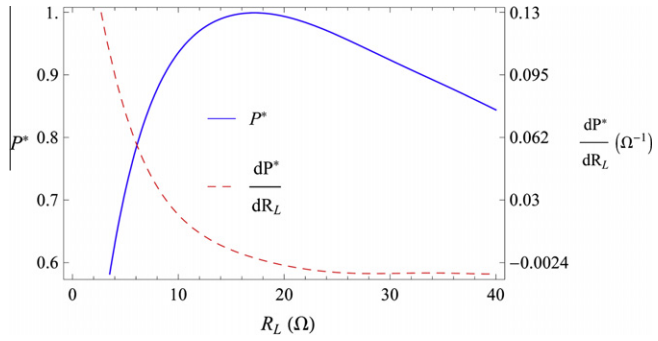

Fig. 11. Effect of an increasing electrical load resistance on normalized power output and its rate of change relative to the electrical load.

This non-dimensional parameter quantifies the thermal input into the generator as a function of the hot and cold fluid temperatures and flow rates.

Fig. 12 compiles the measured peak power measurements from ten test cases. The thermal input conditions vary in temperature difference between the hot and cold sides, hot fluid flow rate and cold fluid flow rate. The peak power points are presented as sets of data in which the thermal input parameters are fixed with exception to either the hot fluid flow rate, the cold fluid flow rate or the temperature difference. The results show that the power output of the tested generator remains within 10% of the value predicted by the non-dimensional term x^* for all thermal input conditions tested. In this way, the peak power output of the generator can be predicted for given thermal input parameters. The results agree with the parabolic behavior relative to temperature and the root function behavior relative to flow rate.

Fig. 13 compares measured $R_{L,opt}$ values to the thermal input conditions in terms of the non-dimensional term x^*. No measurable trends in the $R_{L,opt}$ with respect to the thermal input conditions tested are observed. In particular, the $R_{L,opt}$ is remains within 15% of 15.8 Ω.

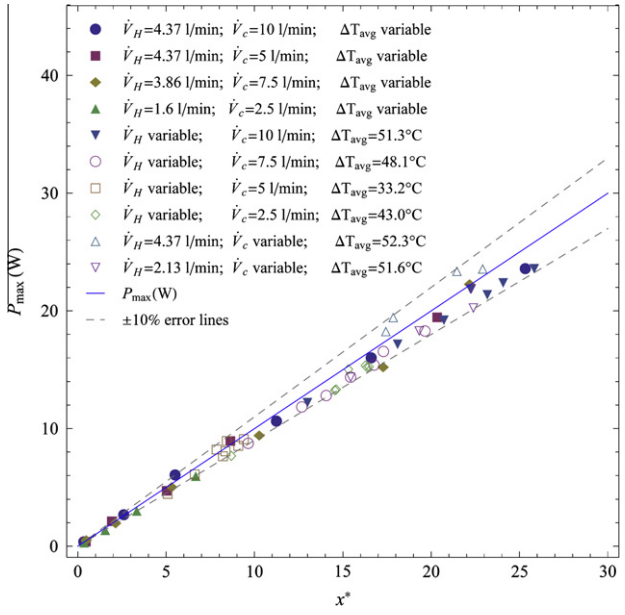

Fig. 12. Peak thermoelectric power for varying thermal input conditions.

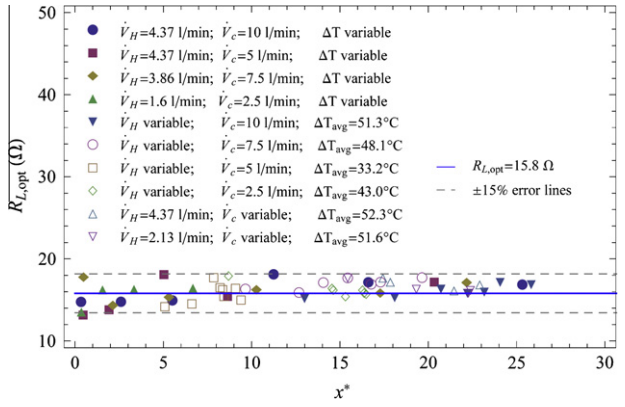

Fig. 13. $R_{L,opt}$ for varying thermal input conditions.

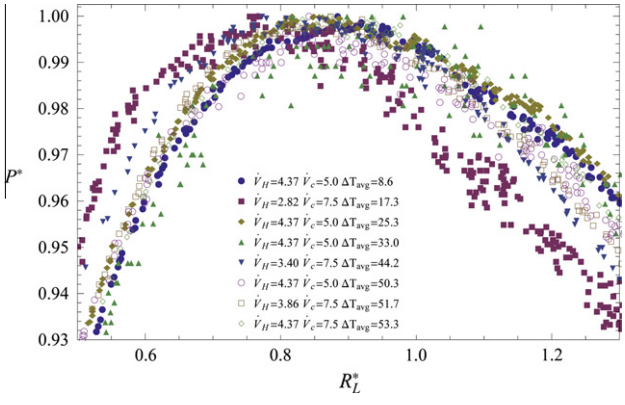

Fig. 14. Effect of dynamically increasing load resistance on normalized power output relative to normalized load resistance.

4.5. Dynamic Load resistance on internal resistance of the generator

The influence of an increasing electrical load is investigated in order to verify the postulation that electrical load matching yields peak thermoelectric power under dynamic conditions. Indeed, the maximum point on the curve generated by Eq. (7) occurs when $R_L = R_{int}$. To this end, from circuit theory, the internal resistance of the generator is calculated by measuring the open circuit voltage [20,23]:

$$R_{int} = \frac{V_{oc}}{I_L} - R_L. \tag{16}$$

The validity of electric load matching for peak power under an increasing load is examined under conditions in which the thermal input varies with varying hot fluid flow, cold fluid flow and temperature. The results are illustrated in Fig. 14. The flow rates are expressed in L/min and the temperatures in °C. The electrical load resistance is increased at a rate of 5.8 ± 2.2 Ω/s.

Fig. 14 shows that, for all thermal conditions tested, electrical load matching yields a minimum of 97.6% peak power. The near peak performance is attributed to the fact that the measured $R_{L,opt}$ is less than the internal resistance of the generator. For this reason, the electrical load matching implies a load resistance that is necessarily greater than optimal which, as illustrated in Fig. 11, is a more forgiving error than an electrical load that is less than optimal; this is due to a relatively small power rate of change with respect to electrical load. Indeed, it is shown in Fig. 15 that the optimal value of R_L^* is strictly less than one ranging from 0.76 to 0.92.

The results presented in Fig. 15 are consistent with the observations made in [13] on a single thermoelectric module in which the optimal electrical load produced from Eq. (16) was strictly greater than the measured optimal load.

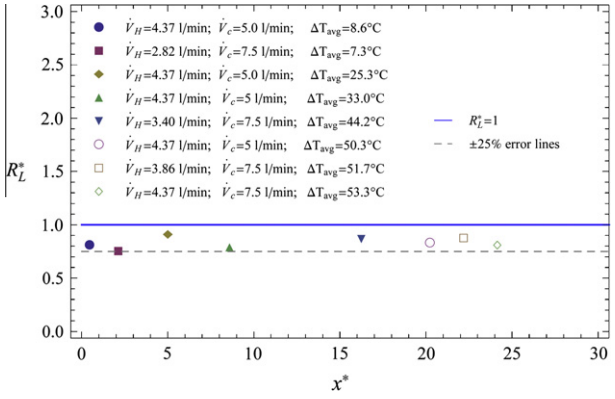

Fig. 15. R_L^* for varying thermal input conditions.

5. Conclusion

A forty module thermoelectric liquid-to-liquid generator is used to measure thermoelectric power production under an increasing electrical load resistance. Varying thermal conditions show that power output behaves exponentially relative to temperature and as a root function relative to fluid flow. The thermal input conditions are quantified in terms of a non-dimensional term that incorporates flow rates and temperatures. A correlation is developed predicting peak power output to within a 10% error margin. The optimal electrical load resistance remained within 15% of 15.8 Ω for all thermal input conditions tested yielding a minimum of 99.0% of the measurable peak power and making an MPPT unnecessary for many applications. Furthermore, it is shown that thermoelectric power production is less sensitive to electrical load error when the load is greater than optimal rather than less than optimal. Since it is also shown that electrical load matching consistently generates electrical loads that are greater than optimal, load matching is deemed in a zone less sensitive to error yielding 97% or

more of the measurable peak power for all thermal input conditions tested.

Acknowledgments

We gratefully thank Marc Desnauliers and Kruger Products for their valuable support throughout this project. We thank the Cégep de l'Outaouais for the 2011 summer grant on thermoelectric power production.

References

[1] Crane DT, Bell LE. Progress towards the performance of a thermoelectric power generator. In: 2006 International conference on thermoelectrics; 2006. 1-4244-0811-3/06.
[2] Kajikawa T, Onishi T. Development for advanced thermoelectric conversion systems. In: 2007 International conference on thermoelectrics; 2008. 978-1-4244-2263-0/08.
[3] Karabetoglu S, Sisman A, Faith Ozturk Z, Sahin T. Characterization of a thermoelectric generator at low temperatures. Energy Conv Manage 2012;62:47–50.
[4] Crane DT, Jackson GS. Optimization of cross flow heat exchangers for thermoelectric waste heat recovery. Energy Conv Manage 2004;45:1565–82.
[5] Rodriguez A, Vian JG, Astrain D, Martinez A. Study of thermoelectric systems applied to electric power generation. Energy Conv Manage 2009;50:1236–43.
[6] Whalena SA, Dykhuizenb RC. Thermoelectric energy harvesting from diurnal heat flow in the upper soil layer. Energy Conv Manage 2012;64:397–402.
[7] Gou X, Xiao H, Yang S. Modeling, experimental study and optimization on low-temperature waste heat thermoelectric generator system. Appl Energy 2010;87:3131–6.
[8] Wee D. Analysis of thermoelectric energy conversion efficiency with linear and nonlinear temperature dependence in material properties. Energy Conv Manage 2012;52:3383–90.
[9] Bélanger S, Gosselin L. Thermoelectric generator sandwiched in a crossflow heat exchanger with optimal connectivity between modules. Energy Conv Manage 2012;52:2911–8.
[10] Hsiao YY, Chang WC, Chen SL. A mathematic model of thermoelectric module with applications on waste heat recovery from automobile engine. Energy 2010;35:1447–54.
[11] Karri MA, Thacher EF, Helenbrook BT. Exhaust energy conversion by thermoelectric generator: two case studies. Energy Conv Manage 2011;52:1596–611.
[12] Hsu C-T, Huang G-Y, Chu H-S, Yu B, Yao D-J. Experiments and simulations on low-temperature waste heat harvesting system by thermoelectric power generators. Appl Energy 2011;88:1291–7.
[13] O'Shaughnessy SM, Deasy MJ, Kinsella CE, Doyle JV, Robinson AJ. Small scale electricity generation from a portable biomass cookstove: prototype design and preliminary results. Appl Energy 2012. http://dx.doi.org/10.1016/j.apenergy.2012.07.03.
[14] Yazawa K, Shakouri A. System optimization of hot water concentrated solar thermoelectric generation. Therm Issues Emerg Technol 2010. IEEE ThETA3_056 283.
[15] Crane DT, Bell LE. Design to maximize performance of a thermoelectric power generator with a dynamic thermal power source. J Energy Res Technol 2009;131:012401-1–1-8.
[16] Hsu C-T, Huang G-Y, Chu H-S, Yu B, Yao D-J. An effective Seebeck coefficient obtained by experimental results of a thermoelectric generator module. Appl Energy 2011;88:5173–9.
[17] Dai D, Zhou Y, Liu J. Liquid metal based thermoelectric generation system for waste heat recovery. Renew Energy 2011;36:3530–6.
[18] Hodes M. On one-dimensional analysis of thermoelectric modules [TEMs]. IEEE Trans Comp Packag Technol 2005;28:218–29.
[19] Rowe DM. Thermoelectrics handbook macro to nano. Taylor & Francis, Group; 2006.
[20] Eakburanawat J, Boonyaroonate I. Development of a thermoelectric battery-charger with microcontroller-based maximum power point tracking technique. Appl Energy 2006;83:687–704.
[21] Lesage FJ, Rousse D. Étude expérimentale sur la résistance externe optimale d'un générateur thermoélectrique. Récents Progrès en Génie des Procédés; 2011. 101-ISBN 2-910239-75-6, Ed. SFGP, Paris (France).
[22] Niu X, Yu J, Wang S. Experimental study on low-temperature waste heat thermoelectric generator. J Power Sources 2009;188:621–6.
[23] Ahiska R, Dislitas S, Omer G. A new method and computer-controlled system for measuring the time constant of real thermoelectric modules. Energy Conv Manage 2012;53:314–21.